INTERIM REPORT TO THE U.S. NUCLEAR REGULATORY COMMISSION

CENTRAL AND EASTERN UNITED STATES SEISMIC SOURCE ZONES AND EARTHQUAKE CHARACTERISTICS - TASK 1

NRC Job Code N6501

Liquefaction Probability Curves for Surficial Geologic Deposits

Thomas L. Holzer
Thomas E. Noce
Michael J. Bennett

U.S. Geological Survey
345 Middlefield Road, MS 977
Menlo Park, CA 94025

e-mail: tholzer@usgs.gov
Phone: (650) 329-5637

January 5, 2010

Liquefaction Probability Curves for Surficial Geologic Deposits

Thomas L. Holzer, Thomas E. Noce, and Michael J. Bennett
U.S. Geological Survey, Menlo Park, CA 94025

Abstract

Liquefaction probability curves that predict the probability of surface manifestations of earthquake-induced liquefaction are developed for 14 different types of surficial geologic units. The units include alluvial fan, beach ridge, river delta topset and foreset beds, eolian dune, point bar, floodbasin, natural river and alluvial fan levees, abandoned river channel, deep-water lake, lagoonal, sandy artificial fill, and valley train deposits. Probability is conditioned on earthquake magnitude and peak ground acceleration. Curves are developed for water table depths of 1.5 and 5.0 m. Probabilities are derived from complementary cumulative frequency distributions of the liquefaction potential index (LPI) that were computed from 935 cone penetration tests. For natural deposits with a water table at 1.5 m and subjected to an **M**7.5 earthquake with a PGA = 0.25 g, probabilities range from <0.03 for alluvial fan and lacustrine deposits to >0.5 for beach ridge, point bar, and deltaic deposits. The curves also were used to assign ranges of liquefaction probabilities to the susceptibility categories proposed by Youd and Perkins (1978) for different geologic deposits. For the earthquake described above, probabilities range from 0-0.08 for low, 0.09-0.30 for moderate, 0.31-0.62 for high, to 0.63-1.00 for very high susceptibility. Retrospective predictions of liquefaction during historical earthquakes based on the curves compare favorably to observations.

Introduction

Most regional mapping of earthquake-induced liquefaction hazard is primarily descriptive and qualitative in nature despite its evolution during the last few decades from research to regulatory endeavors. By contrast, regional mapping of earthquake shaking hazard is typically quantitative. In fact, probabilistic mapping of shaking, which was originally proposed by Cornell (1968), is now firmly established and widely used in engineering practice (McGuire, 2004). The methodology, known as probabilistic seismic hazard analysis, is the basis for estimating shaking hazard in many building codes (Building Seismic Safety Council, 2003; Petersen and others, 2008).

The absence of a widely accepted engineering demand parameter, i.e., a liquefaction intensity parameter that measures the overall severity of liquefaction at a site, is a major obstacle to the implementation of a similar framework for probabilistic liquefaction hazard mapping. Recently, several investigators have produced probabilistic liquefaction hazard maps for earthquake scenarios that use a parameter known as the liquefaction potential index (LPI) as an intensity parameter (see Holzer, 2008 for a review). In the approach developed by Holzer and others (2002; 2006b; 2009), LPI is used to develop liquefaction probability curves for mappable surficial geologic units. These curves predict the probability of surface manifestations of liquefaction for surficial geologic units for a specified water table depth (WT) conditioned on earthquake moment magnitude (**M**) and peak ground acceleration (PGA).

This paper presents liquefaction probability curves for 14 different types of surficial geologic deposits (Table 1). The curves are based on 935 cone penetration test (CPT) soundings that were conducted in these deposits. Many of the deposits are the principal types in which liquefaction has occurred in historical earthquakes (Youd and Hoose, 1977). This paper refines the approach introduced by Youd and Perkins (1978), who proposed a descriptive classification of liquefaction susceptibility of different sedimentary deposits on the basis of their geology and age. They recognized that sedimentary processes responsible for deposition of geologic deposits and the subsequent geologic history can strongly influence liquefaction susceptibility. Liquefaction susceptibility rankings of geologic deposits are often modified with local geotechnical and historical liquefaction frequency data (e.g., Tinsley and others, 1985; Baise and others, 2006; Witter and others, 2006), but the combination does not yield robust estimates of the probability of liquefaction of geologic deposits for different seismic loadings.

Liquefaction probability curves have two primary practical applications. First, the curves can be combined with seismic source characterizations to transform surficial geologic maps into probabilistic liquefaction hazard maps (Cramer and others, 2008; Holzer and others, 2009). Geographic specific curves are clearly preferable, but in the absence of such information, generic liquefaction probability curves provide a first approximation of liquefaction hazard. Such maps are useful both to delineate regional liquefaction hazard and to develop regulatory hazard zones. Second, the curves enable preliminary estimates of liquefaction hazard along paths of lifelines. Lifelines typically cross multiple types of surficial geologic deposits. Liquefaction probability curves can be used to estimate the likelihood of liquefaction during the lifetime of these engineered structures.

Study Areas

Fourteen different types of geologic deposits in 16 study areas were investigated (Table 1 and Figure 1). Six different floodplains were explored because liquefaction is common in this geologic environment. Point bar, floodbasin, abandoned river channel, and natural levee deposits were explored in the floodplain environment. The other types of geologic environments that were explored include beach ridges, alluvial fans, sandy artificial fill, eolian dune, river delta, deep-water lake, coastal lagoon, and valley train. Each type of geologic deposit is described in the section *Liquefaction Probability Curves*.

Three practical considerations influenced selection of study areas. First, one of the research sponsors had an interest in developing a methodology for regionally assessing liquefaction hazard near facilities that it regulates in the central and eastern United States. This prompted us to concentrate on study areas in that part of the country. Second, because the ultimate application of the probability curves is to combine them with surficial geologic maps to produce liquefaction hazard maps, study areas were sought where the surficial geology was mapped. And third, USGS/FEMA Project Impact partnerships facilitated exploration in one of the areas, the greater Oakland area in California, by facilitating permitting. In fact, ease of access and permitting were important considerations in the selection of study areas.

Historical liquefaction has been reported in 6 of the study areas. These are Areas 1, 2, and 15 in the San Francisco Bay region, where liquefaction was observed in earthquakes in 1868, 1906, and 1989; the Mississippi River valley (Areas 8 and 16) in the New Madrid seismic zone, where 3 earthquakes in the winter of 1811-1812 produced widespread liquefaction; and the South Carolina beach ridges (Area 3), where the 1886 Charleston earthquake caused extensive

liquefaction. To avoid introducing a sampling bias in the liquefaction probability curves by oversampling liquefaction sites, field exploration was conducted blindly of known locations of liquefaction. Although the intent of the exploration plan in each of the study areas was to randomly sample surficial units, the design of each plan was dominated by practical considerations, particularly access.

Methodology

Liquefaction Probability

Probabilities of surface manifestations of liquefaction were estimated in this study with the liquefaction potential index (LPI) using the methodology developed by Holzer and others (2002; 2009). The advantage of LPI over the Seed-Idriss simplified procedure (Seed and others, 1985), which only predicts liquefaction potential of a soil element, is that it predicts the liquefaction potential of the entire soil column at a specific location. By combining all of the factors of safety for soil elements in a sounding or boring into a single value, LPI provides a spatially distributed parameter when multiple soundings or borings are conducted in a geologic deposit. The methodology is briefly reviewed here.

LPI was first proposed by Iwasaki and others (1978). It weighs liquefaction factors of safety and thickness of potentially liquefiable layers according to depth at a specific location. Iwasaki and others (1978) assumed that the severity of liquefaction is proportional to:

1. cumulative thickness of the liquefied layers;
2. proximity of liquefied layers to the surface; and
3. amount by which the liquefaction factor safety (*FS*) is less than 1.0, where *FS* is the ratio of the soil capacity to resist liquefaction to seismic demand imposed by the earthquake.

They defined LPI as:

$$LPI = \int_0^{20m} F\, w(z)dz \qquad (1)$$

where

$F = 1 - FS$ for $FS \leq 1$ (2a)

$F = 0$ for $FS > 1$ (2b)

$w(z) = 10 - 0.5\,z$, where z is the depth in meters. (2c)

The weighting factor, *w(z)* ranges from ten at the ground surface to zero at 20 m (Iwasaki and others, 1978). Cohesionless soil above the water table is not subject to liquefaction. LPI takes this into account by assigning *FS>1* at depths above the water table, causing *F*=0 above the water table. LPI values can theoretically range from 0 to 100.

The *FS* used by Iwasaki and others (1978) was based on the "simple analysis" of Iwasaki and others (1982). The boundary curve of their simple analysis, however, differs substantially from that of the Seed-Idriss simplified procedure (Seed and others, 1985); the former generally produces lower Fs values for clean sand as median grain size decreases (Holzer, 2008). In this investigation, *FS* was computed with the simplified procedure as modified for the CPT by Robertson and Wride (1998). This is the CPT procedure recommended by Youd and others

(2001). It is also the procedure that was adopted by Toprak and Holzer (2003) in their calibration of LPI, which was used in this investigation. Their calibration of the significance of LPI was based on correlation of LPI with surface manifestations of liquefaction. They observed that the median values of LPI were 5 and 12, respectively, in areas with sand boils and lateral spreads. Lower and upper quartiles were 3 and 10 for sand boils and 5 and 17 for lateral spreads. The reader is referred to Holzer (2008) for a review of alternative calibrations.

The probability of surface manifestations of liquefaction for each surficial geologic unit is inferred from complementary cumulative frequency distributions of LPI. Distributions are computed for a specific earthquake magnitude, PGA, and water table condition. The probability of liquefaction is the frequency at LPI≥ 5, the empirical threshold value for surface manifestations of liquefaction determined by Toprak and Holzer (2003).

The liquefaction probability methodology is illustrated in Figure 2. Figure 2a shows LPI distributions of young Holocene levee deposits in the Santa Clara Valley, California for a 5-m-deep water table and a **M**7.0 earthquake. Each distribution is based on a specific PGA and the same 25 CPT soundings. The conditional probability of surface manifestations of liquefaction at each PGA is the frequency value at LPI≥ 5 for each distribution. Figure 2b shows liquefaction probabilities inferred from Figure 2a as a function of PGA for an **M**7.0 earthquake.

The probability relation can be generalized to other earthquake magnitudes by scaling the seismic demand, i.e., PGA, by the magnitude scaling factor (MSF) from the simplified procedure (Fig. 2c). The points in Figure 2c are determined from complementary cumulative frequency distributions computed for 5.5≤**M**≤8.0 in 0.5 magnitude increments and 0≤PGA≤0.6 g in 0.1 g increments. In the simplified procedure as described in Youd and others (2001), $MSF = 10^{2.24}/\mathbf{M}^{2.56}$. The probability of surface manifestations of liquefaction (p) is computationally simplified by curve fitting the relation between probability and PGA/MSF. Holzer and others (2006b) recommended the 3-parameter logistic:

$$p = \frac{a}{1+\left(\frac{PGA/MSF}{b}\right)^{c}} \tag{3}$$

Equation (3) is referred to as the liquefaction probability curve of a surficial geologic unit (Holzer, 2008). It is the probability that a surficial geologic unit will exhibit surface manifestations of liquefaction conditioned on PGA and **M**. It is usually computed for a specified water table depth.

In general, a minimum of 25 CPT soundings were conducted to characterize a geologic units. Actual numbers of soundings are shown in Table 1. Soundings generally were spaced one kilometer or greater apart. The number of CPT soundings in a geologic unit that is required to accurately characterize liquefaction potential is an important practical consideration when developing a liquefaction probability curve. The resolution of probability for a specific seismic loading depends on the number of soundings. This is because the probability is inferred from the complementary cumulative frequency distribution of LPI. This is illustrated in Figure 2a, which is based on 25 soundings. The resolution of frequency (and probability) is 4 %. A significant field effort is required to improve resolution because resolution is inversely proportional to the number of soundings. For example, the resolution only improves to 3 % if an additional 8 soundings are performed despite the 32 % increase in field effort. This consideration is more important for geologic units with high liquefaction probabilities than units with low ones.

Case histories, on which the simplified procedure is based and which is used here to estimate *FS*, generally experienced PGA < 0.45 g. For example, only 16 % of the liquefaction

case histories in Moss and others (2006, Table 1) reported PGA > 0.45 g. Although coefficients for equation (3) were computed here that included values of PGA > 0.45 g, the reliability of the liquefaction probability curves at these higher values is unclear. Thus, curves in Figures 2b and 2c are dashed at high values.

Limitations of CPT Simplified Procedure

A convenient advantage of the Robertson and Wride (1998) simplified procedure is that it does not require soil samples for liquefaction evaluation. It only requires measurements of penetration resistance. The procedure relies on the soil behavior index (I_C) to classify soil behavior types and to identify nonliquefiable soil. Although we have found the procedure is fairly reliable when dealing with sands, its perfunctory application to fine-grained soils can produce misleading results particularly in soils where $I_C \approx 2.6$, which is the boundary between liquefiable and nonliquefiable soils in the procedure. Accordingly, in intervals where soil misclassifications were suspected, spot coring was selectively conducted and grain size and Atterberg limits of the samples were measured. This soil sampling prompted us occasionally to modify the Robertson and Wride (1998) procedure and use $I_C \geq 2.4$ to identify nonsusceptible soils. Typically this was done where I_C values varied around 2.6 with depth and it was inferred both from soils samples and geologic setting that the soil was nonliquefiable. It is noted in the text where this modification was made.

The applicability of the simplified procedure to sandy geologic sediment of pre-Holocene (as well as early Holocene) age is a subject of ongoing research (e.g., Andrus and others, 2009). Published field-based CPT classification charts (as well as SPT-based and shear-wave velocity charts) are mostly based on case histories in young Holocene sediments. In general, cyclic resistance ratio is affected more by aging than is penetration resistance (Lewis and others, 1999), so that penetration resistance may not adequately incorporate aging effects. Although a few investigators have explored the application of aging corrections to penetration tests in older sediments, the reliability of generic age corrections is unclear (see Hayati and others, 2008, for a review). Aging effects also can be destroyed by liquefaction. Post-liquefaction consolidation resets the "geotechnical age" of a sand and causes it to behave as it if were freshly deposited (Leon and others, 2006). The age of most of the sediments explored here was either Holocene or late Pleistocene (<15,000 years old). The beach ridges explored in South Carolina, however, ranged in age from Holocene to 200,000-240,000 years old, and sands this old are generally considered to exhibit aging effects. Although sand aging is a concern for developing liquefaction probability curves for older geologic units, it was generally beyond the scope of the present investigation. Aging is modestly addressed here only with regards to the South Carolina Pleistocene beach ridges and Holocene point bar deposits of different ages in the Mississippi River Valley.

Water Table

Liquefaction probability curves were computed for water table depths of 1.5 and 5.0 m to demonstrate the effect of depth to ground water. These depths were chosen based on the CPT liquefaction case histories compiled by Moss and others (2006, Table 1). The water table was shallower than 5 m at 96 % of the case history sites and shallower than 1.5 m at 41 % of the sites. These percentages compare favorably with the percentages for SPT case histories (94 and 38 %)

compiled by Cetin and others (2004, Tables 5 and 7). The small incidence of case histories with water table depths greater than 5 m suggests that the probability curves for surface manifestations of liquefaction may not be applicable to deep water table conditions.

Liquefaction Probability Curves

Liquefaction probability curves are described in this section for each of the geologic deposits that were explored. Constants for the logistic regressions to the curves are compiled at the end of the section. In addition, geologic descriptions of each of the deposits are briefly summarized. The number of soundings varied significantly among the study areas (Table 1). The variation reflected in part whether or not the study area was part of a broader investigation. For example, the extraordinary large number of soundings in the Santa Clara Valley and greater Oakland area were a result of USGS hazard mapping efforts. For areas where the broader investigations have been completed, published references are cited. Geologic maps with locations of soundings are described by Holzer and others (2010a). The CPT data are available at http://earthquake.usgs.gov/regional/nca/cpt/data/.

The field investigations, with one exception, were conducted in areas where surficial geologic maps were available. The exception was the beach ridges along the shore of Lakes Michigan and Superior (Area 4) where aerial photographs were used to guide exploration. The geologic maps were used both to guide the field exploration and to assign surficial geologic classifications to soundings. The mapped geology was accepted in almost all cases to assign a geologic classification to each sounding. The only exceptions were where a sounding offered compelling evidence that the geologic mapping was incorrect. Occasional disagreement of geologic interpretation between a sounding and a map is not unexpected because surficial geologic mapping typically relies on landscape morphology, aerial photography, and agricultural soil type, rather than extensive subsurface exploration. In addition, surficial delineation of boundaries of geologic units can be subjective where units grade into each other. The surficial geologic maps that were used here are compiled in Table 1.

Alluvial Fan Deposits: Holocene alluvial fan deposits were explored in two areas in the San Francisco Bay Region, CA: the greater Oakland area (Area 1), and the northern Santa Clara Valley (Area 2). The original purpose of the subsurface exploration in both areas was to characterize the liquefaction potential of geologic units for liquefaction hazard mapping (Holzer and others, 2006a; Holzer and others, 2009). Both areas are underlain by coalescing alluvial fans that emanate from local drainages. These fan complexes were active until modern urban development covered the land surface and channelized the modern streams (Sowers, 1993). Witter and others (2006) mapped the surficial geology in both areas, and recognized both spatially widespread units on the fan surface and units locally associated with modern streams on the fan. The upper parts of each fan consist of poorly sorted gravels, sands, and clays. These units were mapped as Qhf and Qhfy, with Qhfy being deposits less than 1,000 years old. Grain size generally decreases downslope and the deposits become progressively more clayey. These finer-grained down-slope units were mapped as Qhff. The predominant units mapped along modern stream courses are levee deposits, which were mapped as Qhl and Qhly. Unit Qhly, which includes young levee deposits (<1,000 years old), was identified in only the Santa Clara Valley. Qhly is found primarily along the two major creeks in the valley. In the central part of the Santa Clara Valley, the average thickness of the Holocene alluvial fan deposits is

approximately 9 m; maximum thickness is 18 m (Holzer and others, 2009). The thickness of the Holocene deposits generally decreases outward from the axis of the Santa Clara Valley as they overlap Pleistocene deposits that crop out around the valley margin. In the greater Oakland area, the thickness of the Holocene fan deposits ranges from about 14.3 m to zero where the deposits overlap Pleistocene age sediments (Holzer and others, 2006a); average thickness is about 4.4 m.

Liquefaction probability curves for both alluvial fans are shown in Figure 3. A total of 92 soundings were conducted in Holocene alluvial fan deposits in the greater Oakland area. Liquefaction probabilities for the three major Holocene surficial geologic units–Qhf, Qhff, and Qhl–were similar so the units were lumped together for the purpose of computing a liquefaction probability curve. A total of 123 soundings were conducted in the Holocene alluvial fan deposits of the Santa Clara Valley. As in greater Oakland area, liquefaction potential of the surficial units was comparable except for the young Holocene levee deposits (Qhly) (Holzer and others, 2009). Accordingly, all of the Holocene alluvial fan units except Qhly were lumped together to produce one liquefaction probability curve (Figure 3). Curves for the Santa Clara Valley were originally published by Holzer and others (2009), to which the reader is referred for a more complete discussion. On the basis of soil samples, Holzer and others (2009) used $I_C \geq 2.4$ to identify nonsusceptible soil in the computation of LPI values for the Santa Clara Valley. Similarly on the basis of soil samples, Holzer and others (2010b) applied the same I_C criterion to identify nonsusceptible soil in the greater Oakland area.

Beach Ridges: Subsurface exploration of beach ridges was conducted in two regions: the South Carolina Coastal Plain near Charleston (Area 3), and the Michigan shore of the Great Lakes (Area 4).

The beach ridges in South Carolina were selected because: (1) high-quality surficial geologic mapping was available (Table 1), and (2) liquefaction was observed in parts of these deposits during the 1886 Charleston (**M**7.3) earthquake. The geologic maps delineate 5 regional Pleistocene terrace complexes that formed during interglacial high-sea-level stands. Each complex consists of backbarrier (lagoonal), barrier island (beach ridge), and shallow-ocean-marine-shelf deposits. The terrace complexes were preserved because Quaternary regional crustal uplift of 0.018 mm/yr elevated each complex during intervening glacial low-sea-level stands, which prevented their erosion and destruction during all subsequent interglacial high-sea-level stands (Weems and Lemon, 1993). As a result of the steady uplift, terrace complexes are younger coastward. One hundred CPT soundings were conducted in areas mapped as modern barrier island deposits (Qhs) and barrier island deposits associated with the three youngest Pleistocene terraces. These Pleistocene barrier islands or beach ridge deposits and their ages are: Qts in the Ten Mile-Hill beds (200,000-240,000 yr), Qws in the Wando Formation (70,000-130,000 yr), and Qhes(Qsbs) beneath the Silver Bluff Terrace (33,000-85,000 yr) (Weems and Lemon, 1993). The thickness of the beach ridge units penetrated by the CPT soundings was 5.2±3.1 m. This represents only 37 % of the total thickness of Quaternary deposits, 14.4±4.0 m, in the CPT soundings. The Quaternary deposits rest on Tertiary marine marls and limestones.

Exploration in the Great Lakes region was conducted in three complexes of multiple beach ridges along the shores of Lakes Michigan and Superior (Johnston and others, 2007). The complexes, which are known as strandplains, are associated with prehistorical fluctuations of lake level. According to Thompson and Baedke (1997), each ridge in a strandplain developed in response to approximately 30-year-long cycles of 0.5- to 0.6-m lake-level fluctuations that were superimposed on a late Holocene secular lake-level decline caused by differential post-glacial

isostatic adjustments. Individual beach ridges developed during the high stage of a lake-level fluctuation and increased in width and height during the subsequent cyclic drop of lake level. Because of the ongoing secular decline of lake level associated with the isostatic adjustments, ridges in strandplains, formed in a regular sequential pattern; individual ridges become progressively younger in a lakeward direction. Ages of ridges range from about 1,000 to 4,700 years before the present. According to Johnston and others (2007), a beach ridge typically includes both littoral and eolian sediment, with the eolian deposits underlying the geomorphologically well-expressed ridge. In a study of 5 strandplains along the shore of Lake Michigan by Thompson and Baedke (1997), the number of ridges ranged from about 25 to 100 per strandplain. CPT exploration was conducted in three strandplains: Au Train, Grand Traverse, and Manistique on the Upper Peninsula of Michigan (Figure 1). From 8 to 12 soundings were conducted in each strandplain near the crest of individual ridges. In general, we attempted not to repeatedly penetrate the same beach ridge. Soundings from all of the strandplains were combined to compute a single liquefaction probability curve. The median thickness of the Holocene dune cap as inferred from the CPT soundings was 3.7 (±1.4) m. Of the deposits encountered by each sounding, typically only the beach ridge deposits were susceptible to liquefaction. Other depth intervals were predominantly fine-grained lacustrine deposits.

Liquefaction probabilities for the modern beach ridge and the 3 Pleistocene beach ridges in South Carolina are shown in Figure 4 for both 1.5 and 5.0 m deep water tables. The liquefaction probability curves for the Holocene and Pleistocene beach ridges are similar at lower levels of seismic demand (Figures 4a and b). An interesting aspect of the probability curves at higher seismic demand is that the probabilities of the Pleistocene ridges are higher than those of the Holocene ridge. This agrees with independent studies by Balon and Andrus (2006), Leon and others (2006), and Hayati and Andrus (2008a). Because the finding that the Pleistocene beach ridges are as much or even more liquefiable then the Holocene beach ridge is counterintuitive, we applied an aging factor to the Pleistocene beach ridge curves. Leon and others (2006) concluded that aging caused an average increase of 60 % in resistance to liquefaction of Pleistocene beach ridges in South Carolina, which compares favorably to the 80 % increase reported by Hayati and Andrus (2008a) for the Pleistocene Wando Formation beach ridge (Qws) in Charleston. Accordingly, we multiplied PGA/MSF values for the Pleistocene beach ridge in Figures 4a and 4b by 1.6 to incorporate the effect of aging (Figure 4c and d). This aging correction or aging factor (K_{DR}) at least produces predictions that the younger Holocene beach ridge is more prone to liquefaction than the older Pleistocene beach ridges, which is a more intuitive result. To compute the dashed logistic curve in both Figure 4c and d, the points for all of the Pleistocene beach ridges were lumped together. The single curve fits all three Pleistocene beach ridges for PGA/MSF < 0.3. It should be noted that Hayati and Andrus (2008a) concluded on the basis of extensive liquefaction of Qsbs and Qts in 1886 that an aging factor should be applied only to Qws.

When computing LPI values for each CPT sounding in South Carolina, it was noted that underlying Tertiary age formations contributed about 18 % of the LPI at high levels of ground shaking. The geologic age, high shear-wave velocity (371±122 m/s), and calcareous nature of these marl formations suggest that these soils are not liquefiable and application of the simplified procedure to these sediments is inappropriate. Accordingly, $FS > 1$ were assigned to Tertiary formations in the CPT profiles and LPI values were then recomputed. This approach is supported by liquefaction susceptibility studies of the marl by Li and others (2007) and Hayati and Andrus (2008b).

Liquefaction probabilities of the beach ridges that were explored along the Great Lakes are shown Figure 5. Probabilities are significantly smaller than are the probabilities of the South Carolina beach ridges. In addition, the impact of a deeper water table, i.e., 5 m, is more pronounced. Both effects are the result of the smaller thickness of the beach ridges in the Great Lakes.

Deltaic and Lacustrine Deposits: Subsurface exploration was conducted in Richland County, North Dakota, at the southern margin of the plain created by former proglacial Lake Agassiz (Areas 5 and 14). The geology of the lake deposits is described by both Baker (1966) and Arndt (1977). The lake occupied part of the modern Red River Valley between about 9,000 and 13,800 years ago when the continental Laurentide ice sheet created a large ice dam in the valley (Arndt, 1977). Surface water runoff, which naturally flowed northward in the valley, was impounded by this giant ice sheet. The lake survived until the ice dam disappeared. The lake at its maximum extent covered approximately 1,500,000 km^2 (Teller and Leverington, 2004). During the lake's terminal phase as the ice sheet waned, it is believed to have drained catastrophically through the ice dam in a series of large outbursts. The largest and youngest outburst occurred approximately 8,400 years ago according to Teller and Leverington (2004), which implies the lake lasted a little longer than inferred by Arndt (1977).

Both coarse-grained deltaic sediment deposited by the Sheyenne River (Area 5) in the proglacial lake and fine-grained deep-water lake deposits (Area 14) were explored. Baker (1966) identified two deltaic facies. Both facies are readily recognized in the CPT soundings, and can be distinguished based on penetration resistance and bedding thickness. The two deltaic facies are sandy topset beds that were deposited where the river discharged into the lake and silty foreset beds that were deposited along the advancing front of the delta in Lake Agassiz. Arndt (1977) dated the age range of the deltaic deposits as from 12,000 to 13,800 years old. The deep-water lacustrine facies predominantly consists of fat clays (CH) with a plasticity index that ranges from 25 to 53. We infer that the deep-water deposits are part of Arndt's (1977) Sherack Formation, dated at 9,000 to 9,900 years old.

Liquefaction probability curves for both deltaic facies and the curve for the deep-water lacustrine facies are plotted in Figure 6. The curves indicate the sandy topset facies is more liquefiable than the silty foreset facies. The deep-water lacustrine facies has only a small liquefaction probability. We do not attribute much significance to the low probabilities of the lacustrine facies at PGA/MSF > 0.45 g and a water table depth of 1.5 m, although the small probabilities may be caused in part by the presence of thin silt layers in the otherwise clay-rich environment. An $I_C \geq 2.4$ criterion was adopted to identify nonsusceptible soil in the foreset facies when computing LPI values on the basis of sampling in depth intervals with $2.4 < I_C < 2.6$. Most of the soil samples with I_C values in this range were not susceptible to liquefaction according to the Bray and Sancio (2006) criteria. As a practical matter, normalized penetration resistance values for many of the sampled intervals plotted in soil zone 4 (silt mixture) on the Robertson and Wride (1998) soil behavior type chart in the part of the chart where the $I_C \geq 2.6$ criterion misclassifies the soil type as zone 5 (sand mixture), which is susceptible. Holzer and others (2008) showed that the boundary in this part of the chart is better fit with the $I_C \geq 2.4$ criterion. Application of the $I_C \geq 2.4$ criterion to the CPT soundings in the foreset facies reduced probabilities by approximately 50 %.

Eolian Dunes: Wind-blown or eolian dunes were explored in Indiana Dunes National Lakeshore along the southern shore of Lake Michigan (Area 6). The surficial and shallow subsurface geology of the area is described by Thompson (1990). The eolian deposits consist of moderate- to well-sorted, in a geologic sense, fine-grained sand (median grain size diameter, d_{50} = 0.14 to 0.31 mm). Although surficial exposures of the dunes indicate deposition by wind, subsurface investigations indicate that the dunes are a dune and beach complex that is interbedded with swamp, lake, and shoreline deposits associated with Holocene water-level fluctuations of Lake Michigan. Such sedimentary complexity is typical of dune fields because dunes typically migrate laterally in response to wind changes and bury adjacent noneolian sedimentary deposits during the migration. Although the dune field is presently active and thus of young Holocene age, sediments in the dune complex are up to 6,000 years old according to Thompson (1990). The total thickness of dune deposits penetrated by the USGS soundings ranged from 3.5 to greater than 20.5 m. Average thickness was 10.9 m. Tip resistance and shear-wave velocity were lower in the upper part of each sounding, which we infer to be of younger Holocene age and the active part of the dune. The thickness of the younger upper interval in the soundings was 6.4±2.8 m. In general, this interval contributed most of the LPI.

Floodplains: The most extensive subsurface exploration of this investigation was conducted in 6 floodplains. The focus was on point bar deposits, although some exploration was conducted in other floodplain facies. Point bar deposits are commonly implicated in post-earthquake liquefaction investigations of liquefaction (e.g., Dupré and Tinsley, 1998). In addition, liquefaction was widespread in point bar deposits in the northern part of Area 8 during the 1811-1812 New Madrid earthquakes. In simple terms, point bars are sandy and silty sediments that are deposited at high stream stages along the inside bend or convex side of a laterally migrating stream channel.

Point bar deposits were explored in 5 of the 6 floodplains (Table 1). All 5 floodplains are associated with low-gradient meandering river courses. However, the sizes of the contributing drainage basins–the area of the drainage basin upstream from the study area–vary by 3 orders of magnitude (Table 2). The largest drainage basin is the Mississippi River with a contributing drainage basin area of 2,414,908 km^2; the smallest is the Wolf River, near Memphis, TN, with an area of only 1,836 km^2.

Exploration of point bar deposits in the Mississippi River Valley (Area 8) was conducted from 207 to 78 km, respectively, northeast and southwest of Memphis, TN. Saucier (1994a) subdivided Holocene point bar deposits in the Mississippi River Valley into 6 different sequences based on their age. The youngest is Hpm1, which underlies the currently active floodplain, and the oldest is Hpm6, which is in the floodplain that was active in the early Holocene. Exploration was conducted in Hpm1 to Hpm5. Their chronologic ages will be discussed later in this section. The other 4 point bar locations that were explored are in the active floodplains of the Ouachita River south of Camden, AK (Area 9), the Red River near Texarkana, AK (Area 10), the Rio Grande, northwest of Brownsville, TX (Area 11), and the Wolf River, east of Memphis, TN (Area 12). Exploration in each of these 4 floodplains was conducted along reaches of the rivers that ranged in length from 23 to 57 km.

Liquefaction probability curves for all 5 point bar deposits are shown in Figure 8. Only the curve for Hpm1 is plotted for the Mississippi River floodplain. The curves for the different areas are remarkably comparable, with a total range of probability of only about 0.2 at higher values of PGA/MSF. This comparability is most likely a consequence of the similarity of rivers.

They are all meandering rivers. Liquefaction potential does not appear to be strongly correlated with the size of the contributing drainage basin.

Limited exploration of floodbasin, abandoned channel, and natural river levee deposits was conducted in the floodplains of the Mississippi (Area 8) and Ohio Rivers (Area 7). Floodbasin (or backswamp) deposits are fine-grained overbank flood facies typically consisting of silt and clay-rich sediments that are laid down in slack-water environments associated with floods. Abandoned channel deposits, as the name implies, are sediments laid down in former reaches of river channels. Natural river levee deposits are coarser-grained sediments that are laid down adjacent to the river channel when banks are overtopped during flood stage.

Floodbasin and abandoned channel deposits were explored in the Mississippi River floodplain (Area 8). Floodbasin deposits, which Saucier (1994b) mapped as unit Hb, underlie a large portion of the modern Mississippi River floodplain, particularly south of Memphis, TN. These floodbasins were important centers of deposition during flooding before humans constructed levees along the river channel. Abandoned channel deposits, which Saucier (1994b) mapped as Hchm, are incised into point bar deposits. According to Saucier (1994a), most of these channels were abandoned as the result of "neck cutoffs," which occur when two bends in the river meander and intersect. The abandoned river channel, which then becomes an oxbow lake, typically undergoes a predictable cycle of sediment infilling. Initially, the lake may remain partly connected to the river, which continues to deposit some silts and sands in the lake. When the channel becomes completely isolated from the river, sediment fill becomes finer grained. This fine-grained fill is known to engineers as a "clay plug." "Chute cutoffs," which are much less common in the Mississippi River floodplain according to Saucier (1994a), are channels that are abandoned when rivers overflow their banks during floods and scour and create a new channel. Chute cutoffs typically are infilled by a variety of sedimentary processes.

Floodbasin and natural river levee deposits were explored in the greater Evansville, IN, area (Area 7). Evansville lies on the northern bank of the Ohio River. Our field investigation was initially guided by the mapping of Fraser and Fishbaugh (1986), who inferred that the deposits underlying the flat plain north of Evansville were lacustrine. The CPT exploration, however, revealed that these deposits contained two facies: (1) a sandy silt deposit immediately north of a high glacial outwash terrace along the river, and (2) a silty clay deposit further northward. The facies interfinger and their transition is gradational. We concluded that the two facies were the result of overbank deposition during extreme flooding of the Ohio River; the silty clay facies is a floodbasin deposit and the coarser grained facies is a natural river levee deposit. CPT profiles in the floodbasin facies indicate thicker bedding than is typical of lacustrine deposits. In addition, a core sample from a depth of 3.8 m collected in the fine-grained facies by Ron Counts of the Kentucky Geological Survey exhibited cross bedding and contained fossil gastropods, *Gastropoda Pomatiopsis lapidaria*, both of which suggest subaerial floodbasin deposition rather than lacustrine deposition (J.C. Tinsley, pers. comm., 2004). The delineation of the natural river levee deposit is consistent with: (1) grain-size analyses reported by Kayaballi and West (1994, Figures 7 and 8), who described a shallow coarser grained facies north of the glacial outwash terrace, and (2) recently published surficial mapping of the Evansville surficial geology (Moore and others, 2009).

Liquefaction probability curves for floodbasin, abandoned channel, and natural levee deposits are shown in Figures 9 and 10. The floodbasin deposits in the Mississippi River floodplain (Figure 9a) are more liquefiable than those in the Evansville, IN, area (Figure 10a). This probably reflects differences in the relation of the respective floodbasins to the river. The

Evansville deposits are more distal from the river, forming when the Ohio River overtopped a relatively high glacial terrace. Most of the courser grained sediment during overtopping was deposited in the natural levee deposit adjacent to the river (Figure 10b). By contrast floodbasin deposits in the Mississippi River floodplain occasionally bury point bar deposits. These buried deposits enhance liquefaction potential in areas mapped as floodbasin, which reflects a more recent geologic setting. The high liquefaction probabilities of the abandoned channel deposits (Figure 9b) presumably are a consequence of their complex fill histories, which include deposition of point bar and channel sands particularly in the early stages of channel abandonment.

The limited exploration of point bar deposits of different Holocene ages in the Mississippi River floodplain permits a modest evaluation of the effect of aging (Figure 11). Saucier (1994a) estimated the 5 abandoned floodplains to range in age from 2,600 to 10,000 years old. Exploration was conducted in point bar deposits in three of these abandoned floodplains. In order of increasing age, they were mapped by Saucier (1994a) as units Hpm3, Hpm4, and Hpm5. Units Hpm3 and Hpm4, which were lumped together, range in age from 3,800 to 6,500. Unit Hpm5 ranges in age from 7,000 to 9,200 years old. Saucier (1994a) estimated that the age of unit Hpm1, the active floodplain point bar facies, is less than 3,000 years old. There is not a systematic ordering by geologic age of the probability curves in Figure 11 for the different point bars.

Lagoonal Deposits (Backbarrier): Exploration was conducted in the lagoons and marshes along an 80-km long reach of the Texas coast in Brazoria and Matagorda Counties. The area lies inland of the barrier island that forms the modern shoreline. The modern coastal environment began to evolve when sea level reached its present position in this area between 2,500 and 3,000 years ago (McGowen and others, 1976). The lagoonal and marsh deposits described here are basically a coeval coastal facies with the barrier island or beach ridge facies (McGowen and others, 1976). The lagoonal facies is sometimes referred to as backbarrier. Depositional processes in the backbarrier environment range from quiet shallow water deposition to organic soil accumulation to sandy storm-driven washover and storm-breach channel sedimentation. Washovers typically are caused by hurricane storm surges that transport beach sand across the barrier island and into the lagoonal and marsh areas, where they may be subsequently buried by quiet water fine-grained deposits. In addition, coarse-grained sediments sediments may be deposited by streams and rivers where they transect the marshes and lagoons, as well as by flood tides passing through tidal passes (natural breaks in the barrier islands). As a consequence of the multitude of active processes, stratigraphy in the backbarrier environment often is complex.

Liquefaction probability curves for the lagoonal deposits are shown in Figure 12. The soundings encountered a large amount of susceptible sand in this environment, and this is reflected in the probability curves.

Sandy Artificial Fills: Only one artificial fill, the sandy fills along the waterfront of greater Oakland on the east shore of San Francisco Bay, California (Area 15), was explored. Eighty-two CPT soundings were conducted in these fills as part of a regional liquefaction hazard mapping effort (Holzer and others, 2006a). The fills underlie an area of 57 km^2, which represents 22 % of marshland and tidal and submerged land that has been reclaimed from San Francisco Bay since 1847 (USDC, 1959). Fill thickness ranges from zero, where the fill pinches out along the original shoreline, to about 11 m; average thickness is about 3 m (Holzer and others, 2006b).

Most of the east bay fill was placed after 1906, often by hydraulic dredging of sand (Rogers and Figuers, 1991). The largest individual fill, six million cubic meters, was placed between January 1941 and June 1942 to create military facilities during World War II. With the exception of the 1989 Loma Prieta (**M**6.9) earthquake (Holzer, 1998), the post-1906 fills have not been subjected to strong shaking and liquefaction.

Liquefaction probability curves for the sandy artificial fill are shown in Figure 13. Because the fills were placed before 1964 when liquefaction as an engineering hazard was broadly recognized, most were placed without consideration for their vulnerability to liquefaction. Small portions of the fills, however, at some sites were subsequently improved.

Valley Train Deposits: Subsurface exploration of valley train deposits was conducted in the Mississippi Valley in Arkansas and Missouri (Area 16). Valley train deposits are laid down by sediment-laden runoff from melting glaciers. In the Mississippi Valley, they were deposited by braided streams fed by the ablation of the continental Laurentide ice sheet in the Late Wisconsin and early Holocene (Saucier, 1994a). Exploration was focused on the two geologically youngest units mapped by Saucier (1994a), Pvl1 and Pvl2. Pvl1 is approximately 10,000 years old. It records the youngest discharge of sediment-laden glacial melt water down the Mississippi Valley. Pvl2 is older. It records an earlier discharge pulse. Pvl2 may be older than 12,000 years on the basis of artifacts from Paleo-Indian cultures. Comparison of liquefaction effects maps by Obermeier (1989) with the geologic maps by Saucier (1994b) indicates extensive liquefaction of Pvl1 and Pvl2 during the 1811-1812 New Madrid earthquake sequence. The comparison indicates approximately 64 % of the 1811-12 liquefaction area is underlain by these valley train deposits.

The liquefaction probability curves of the two valley train deposits differ particularly at high values of PGA/MSF, with Pvl2 exhibiting significantly higher probabilities. At lower values of PGA/MSF, Pvl1 exhibits slightly higher probabilities.

Constants for Equation (3): Constants for the 3-parameter logistic presented in the figures in this section for all of the surficial geologic units are compiled in Table 3. Constants are based on a regression of $0<PGA/MSF<0.7$. Correlation coefficients in general were greater than 0.98. As can be seen in some of the figures, the regression often is poorest at PGA/MSF values where liquefaction probabilities just start to increase from zero. When ground motions are primarily in this range, a regression to only the ground-motion in the range of interest may more rigorously capture the relation.

Discussion

Retrospective predictions of liquefaction occurrence in historical earthquakes in the San Francisco Bay area, California, which can be compared to post-earthquake observations, constitute our primary effort to validate the liquefaction probability curves presented here. Liquefaction hazard maps were prepared for parts of the Bay area where liquefaction was observed in earthquakes in 1868, 1906, and 1989 (Holzer and others, 2006b; Holzer and others, 2009, 2010b). The hazard maps present liquefaction scenarios for reoccurrences of these earthquakes. The comparison of predicted and historical observations in general is favorable. Comparisons are most complete for the 1989 (**M**6.9) Loma Prieta earthquake for which liquefaction effects were thoroughly documented (Holzer, 1998). For this earthquake, 14 % of

the area underlain by sandy artificial fill in the greater Oakland area was predicted to exhibit surface manifestations of liquefaction, which compares favorably to the observed area of 13 % (Holzer and others, 2006b). Similarly, no liquefaction effects were predicted in susceptible stream deposits in the Santa Clara Valley for the Loma Prieta earthquake, and no effects were observed (Holzer and others, 2009). Liquefaction during the 1868 Hayward Fault (**M**6.7-6.9) and 1906 San Francisco (**M**7.8) earthquakes was less thoroughly documented, but observed effects are consistent with predicted effects (Holzer and others, 2009, 2010b).

In addition to these comparisons, probabilities predicted with the curves generally agree with historical experience. This experience includes the extensive liquefaction of floodplain deposits associated with the 1964 Niigata, Japan, **M**7.5 (Kawasumi, 1968) and 1811-12 New Madrid ~**M**7.5-7.7 earthquakes (Obermeier, 1989), the widespread liquefaction of sandy artificial fills during the 1975 Hyogoken-Nambu (Kobe), Japan, **M**7.2 (Hamada and others, 1995) and 1906 San Francisco earthquakes (Youd and Hoose, 1978), and the limited liquefaction of alluvial fan deposits during the 1994 Northridge **M**6.7 earthquake (Holzer and others, 1999).

The ultimate testing and validation of the liquefaction probability curves, however, will be by thorough documentation of field occurrences of liquefaction during future post-earthquake investigations of large earthquakes in liquefaction-prone areas. The probability of liquefaction equals the percent area affected by liquefaction (Holzer, 2008). Thus, meticulous post-earthquake mapping of surficial manifestations of liquefaction associated with a surficial geologic deposit can be combined with local ground-motion observations to independently develop liquefaction probability curves for geologic units. Such empirical curves will provide the ultimate test of the validity of the curves developed here, which are inferred from geotechnical properties of geologic deposits.

The liquefaction probability curves can be used to assign probabilities to the descriptive susceptibility ratings proposed by Youd and Perkins (1978) because similar classifications of geologic deposits were used in both investigations. The resulting probabilities also can be used to evaluate the liquefaction probability curve methodology to the extent that the probabilities assigned to the susceptibilities appear reasonable. A seismic loading must be assumed, however. Estimates of probability are presented in Figure 15, where probabilities for each surficial geologic deposit were computed for an **M**7.5 earthquake and a PGA = 0.25 g, and a water table depth of 1.5 m. This seismic loading was chosen because an **M**7.5 earthquake is the reference earthquake in the simplified procedure and the preponderance of case histories are for earthquakes with **M** ≤ 7.5. PGA = 0.25 g is the mode of the ground motions in the case histories compiled by Moss and others (2006). We assume that this earthquake and shallow water table approximate a "worst case" scenario condition. The susceptibility ratings plotted on the abscissa are from the Holocene deposit column in Table 2 of Youd and Perkins (1978). Estimated liquefaction probabilities in Figure 15 generally are small for susceptibility ratings of low and very low, and increase as susceptibility rating increases from moderate to very high. The hand drawn curve in Figure 15 is intended to illustrate the trend. To draw the curve, we assumed that the upper range of "very high" susceptibility should correspond to a $p = 1.0$. Table 4 (column 1) shows probability ranges for each susceptibility category inferred from the hand drawn curve in Figure 15. Table 4 also shows probability ranges for a deeper water table and smaller earthquake. Probabilities are significantly smaller for both a 5-m-deep water table with the same earthquake loading and a 1.5-m-deep water table and a smaller magnitude (**M**6) earthquake (Table 4).

The range of probabilities for the geologic deposits in each susceptibility rating category in Figure 15 is large, but not unexpected. Although it might be caused in part by

misclassifications of susceptibility by Youd and Perkins (1978), the range presumably also reflects real differences of liquefaction potential among geologic deposits of similar type. Two geologic factors can contribute to the range of probabilities: (1) sedimentation variability, and (2) differences of thickness.

Sedimentation variability is caused by the spatial dynamics of depositional environments. Most of the surficial geologic units investigated here were not deposited in isolation. They were part of an assembly of coeval units where each unit was the product of a particular depositional environment. For example, an active barrier beach ridge environment commonly is bounded by lagoonal and marsh environments on it back side and a shallow marine environment on its oceanic side. Depositional processes substantially differ among the three environments. In addition, the environments may laterally migrate over time. This migration causes heterogeneity of geologic units as well as interfingering of units in the subsurface. A surficial geologic map is only a snap shot of the units at the surface when these environments cease to be active. These maps, absent detailed cross sections, typically do not explicitly portray the subsurface complexity. Thus, geologic complexity can be expected to create variations in liquefaction probability curves from area to area even though surficial geology as mapped may be broadly similar.

Thicknesses of similar types of surficial geologic deposits can differ substantially even where depositional environments are spatially stable. Thickness is determined by factors such as sediment supply and longevity of the particular depositional process. Thickness affects probability because it has a large impact on LPI values (Holzer, 2008). The impact of thickness is demonstrated by comparing liquefaction probability curves for beach ridges in South Carolina with those for the Great Lakes and for alluvial fans in the Santa Clara Valley with those for the greater Oakland area. Liquefaction probabilities are higher for the thicker South Carolina beach ridges and Santa Clara Valley alluvial fans.

The causes of the variability in probability curves for specific types of surficial geologic units are important to understand if the curves are to have broad application. One of the goals of the present research was to develop generic liquefaction probability curves that would enable surficial geologic maps to be transformed into liquefaction hazard maps. Although area-specific geotechnical data are preferable, these data are not always available. Generic probability curves would facilitate transformation of surficial maps. An alternative to single generic curves might be to develop curves for different ranges of sedimentary thickness for each type of geologic deposit. Thickness of the deposits is most likely a major cause of variability. A curve appropriate for the type of geologic unit could then be applied based on average thickness. Information on thickness of surficial geologic units increasingly is being incorporated into the mapping process by modern surficial geologists. Many of these geologists routinely develop three-dimensional conceptualizations of the geology. The maps produced by Weems and his colleagues that describe the surficial geology of the South Carolina Coastal Plain (Table 1) illustrate this trend. Their mapping of the Tertiary surface and published cross sections greatly facilitated our interpretation of the geologic stratigraphy encountered by the CPT soundings.

Finally, the impact of geologic age when using the simplified procedure to compute liquefaction probability curves was only modestly addressed here. Geologic age is an important criterion in the classification of liquefaction susceptibility proposed by Youd and Perkins (1978) as well as a consideration for evaluation of liquefaction potential of pre-Holocene deposits (Andrus and others, 2009). The effect of age on the liquefaction probability curves is difficult to evaluate here because field exploration was primarily focused on variation in the types of

geologic surficial units rather than on variation of age within specific surficial geologic units. Nevertheless, curves for the South Carolina Pleistocene beach ridges and the Mississippi River Holocene point bars permit speculation. The intuitively appealing age corrections to the beach ridges suggest that the Pleistocene beach ridges may be affected by sand aging (Figure 4). The absence of a consistent variation of liquefaction probability with age of the Holocene point bar deposits suggest aging effects at time scales of less than 10,000 years are modest (Figure 11). This is consistent with the summary of sand aging studies by Hayati and others (2008). Although many investigators of aging associate it with an exponential time-dependent process, Hayati and others (2008, p. 8) noted that K_{DR}'s of 1.0 and 2.0, respectively, for Holocene and Pleistocene sediments were a plausible alternative interpretation.

Acknowledgments: This research was made possible by support from several institutions and the generous assistance of many colleagues. This work was funded in part by the U. S. Nuclear Regulatory Commission grant N6501, Central and Eastern States seismic source zones and earthquake characteristics. These findings express the views of the authors and are not necessarily those of the U.S. NRC. Other supporters include the USGS Earthquake Hazards Program and Central United States Earthquake Consortium. Purchase of the CPT truck was partially enabled by the PG&E-USGS CRADA. We are especially grateful to the following individuals for discussions and help: John C. Tinsley, Glenn Rix, David Moore, Scott Lundstrom, Todd Thompson, Norman Hester, Coyn Criley, Buddy Schweig, Kathy Tucker, Rob Weems, Selcuk Toprak, Amy C. Padovani, and Jim Wilkerson. We appreciate reviews of an early draft by Ronald D. Andrus and John C. Tinsley, III. This publication was approved by the Director, USGS, December 29, 2009.

References

Andrus, R.D., Hayati, H., and Mohanan, N.P., 2009, Correcting liquefaction resistance for aged sands using measured to estimated velocity ratio: Journal of Geotechnical and Geoenvironmental Engineering, v. 135, no. 6, p. 735-744.

Arndt, B.M., 1977, Stratigraphy of offshore sediment, Lake Agassiz, North Dakota: North Dakota Geological Survey Report of Investigation No. 60, 58 p.

Baise, L.G., Higgins, R.B., and Brankman, C.M., 2006, Liquefaction hazard mapping-Statistical and spatial characterization of susceptible units: Journal of Geotechnical and Geoenvironmental Engineering, v. 132, no. 6, p. 705-715.

Baker, C.H., Jr., 1966, Geology and Ground Water Resources of Richland County, Part 2-Basic Data: North Dakota State Water Conservation Commission, County Ground Water Studies 7, 80 p.

Balon, D.R., and Andrus, R.D., 2006, Liquefaction potential index of soils in Charleston, South Carolina, based on the 1886 earthquake, Proceedings of the 8th U.S. National Conference on Earthquake Engineering.

Bray, J.D., and Sancio, R.B., 2006, Assessment of the liquefaction susceptibility of fine-grained soils: Journal of Geotechnical and Geoenvironmental Engineering, v. 132, no. 9, p. 1165-1177.

Broughton, A.T., 1999, Geologic and liquefaction susceptibility mapping in the Collierville 7.5 minute topographic quadrangle: Memphis, TN, The University of Memphis, M.S. Thesis, 61 p.

Brown, L.F., Jr., Brewton, J.L., McGowen, J.H., White, W.A., Groat, C.G., and Fisher, W.L., 1980, Environmental geologic atlas of the Texas Coastal Zone: Brownsville-Harlingen area: Texas Bureau of Economic Geology, 140 p.

Building Seismic Safety Council, 2003, NEHRP recommended provisions for seismic regulations for new buildings and other structures, Part 1- Provisions and Part 2- Commentary: Federal Emergency Management Agency.

Cetin, K.O., Seed, R.B., Kiureghian, A.D., Tokimatsu, K., Harder, L.F., Kayen, R.E., and Moss, R.E.S., 2004, Standard penetration test-based probabilistic and deterministic assessment of seismic soil liquefaction potential: Journal of Geotechnical and Geoenvironmental Engineering, v. 130, no. 12, p. 1314-1340.

Cornell, C.A., 1968, Engineering seismic risk analysis: Seismological Society of America Bulletin, v. 58, no. 5, p. 1583-1606.

Cox, R.T., 2004, Surficial geologic map of the northeast Memphis quadrangle, Shelby County, Tennessee, and Crittenden County, Arkansas: U.S. Geological Survey Scientific Investigations Map 2839, scale 1:24,000.

Cramer, C.H., Rix, G.J., and Tucker, K., 2008, Probabilistic liquefaction hazard maps for Memphis, Tennessee: Seismological Research Letters, v. 78, no. 3, p. 416-423.

Dupré, W.R., and Tinsley, J.C., III, 1998, Evaluation of liquefaction hazard mapping in Monterey Bay region, central California, *in* Holzer, T.L., ed., The Loma Prieta, California, earthquake of October 17, 1989 - Liquefaction: U. S. Geological Survey Professional Paper 1551-B, p. B273-B286.

Fisher, W.L., McGowen, J.H., Brown, L.F., Jr., and Groat, C.G., 1972, Environmental geologic atlas of the Texas Coastal Zone: Galveston-Houston area: Texas Bureau of Economic Geology, 91 p.

Fraser, G.S., and Fishbaugh, D.A., 1986, Alluviation of the Ohio River Valley near Evansville, Indiana, and its effect on the distribution of sand and gravel in the area: Indiana Geological Survey Special Report 36, 26 p.

Hamada, M., Isoyama, R., and Wakamatsu, K., 1995, The 1995 Hyogoken-Nanbu (Kobe) earthquake - Liquefaction, ground displacement, and soil condition in the Hanshin area: Tokyo, The School of Science and Engineering, Waseda University, 194 p.

Hayati, H., and Andrus, R.D., 2008a, Liquefaction potential map of Charleston, South Carolina, based on the 1886 earthquake: Journal of Geotechnical and Geoenvironmental Engineering, v. 134, no. 6, p. 815-828.

Hayati, H., and Andrus, R.D., 2008b, Liquefaction susceptibility of fine-grained soils in Charleston, South Carolina, based on CPT, GeoCongress: New Orleans, LA, ASCE.

Hayati, H., Andrus, R.D., Gassman, S.L., Hasek, S.L., Camp, W.M., and Talwani, P., 2008, Characterizing the liquefaction resistance of aged soils, *in* Zeng, D., Manzari, M.T., and Hiltunen, D.R., 4th Geotechnical Earthquake Engineering and Soil Dynamics: Sacramento, CA, ASCE Geotechnical Special Publication 181, p. 1-10.

Holzer, T.L., ed., 1998, The Loma Prieta, California, earthquake of October 17, 1989 - Liquefaction, U.S. Geological Survey Professional Paper 1551-B, 314 p.

Holzer, T.L., 2008, Probabilistic liquefaction hazard mapping, *in* Zeng, D., Manzari, M.T., and Hiltunen, D.R., 4th Geotechnical Earthquake Engineering and Soil Dynamics: Sacramento, CA, ASCE Geotechnical Special Publication 181, p. 1-32.

Holzer, T.L., Bennett, M.J., Noce, T.E., Padovani, A.C., and Tinsley, J.C., III, 2002, Liquefaction hazard and shaking amplification maps of Alameda, Berkeley, Emeryville, Oakland, and Piedmont: A digital database: U.S. Geological Survey Open-file Report 02-296.

Holzer, T.L., Bennett, M.J., Noce, T.E., Padovani, A.C., and Tinsley, J.C., III, 2006a, Liquefaction hazard mapping with LPI in the greater Oakland, California, area: Earthquake Spectra, v. 22, no. 3, p. 693-708.

Holzer, T.L., Bennett, M.J., Ponti, D.J., and Tinsley, J.C., III, 1999, Liquefaction and soil failure during the 1994 Northridge earthquake: Journal of Geotechnical and Geoenvironmental Engineering, v. 125, no. 6, p. 438-452.

Holzer, T.L., Blair, J.L., Noce, T.E., and Bennett, M.J., 2006b, Predicted liquefaction of East Bay fills during a repeat of the 1906 San Francisco earthquake: Earthquake Spectra, v. 22, no. S2, p. S261-S278.

Holzer, T.L., Noce, T.E., and Bennett, M.J., 2009, Scenario liquefaction hazard maps of Santa Clara Valley, Northern California: Seismological Society of America Bulletin, v. 99, no. 1, p. 367-381.

Holzer, T.L., Noce, T.E., and Bennett, M.J., 2010a, Maps and documentation of seismic CPT soundings in the central and eastern United States: U.S. Geological Survey Open-file Report (in press).

Holzer, T.L., Noce, T.E., and Bennett, M.J., 2010b, Predicted liquefaction in the Greater Oakland area and Northern Santa Clara Valley durin a repeat of the 1868 Hayward Fault (**M**6.7-7.0) earthquake, *in* Knudsen, K.L., 3rd Conference on earthquake hazards in the eastern San Francisco Bay Area, p. in press.

Iwasaki, T., Tatsuoka, F., Tokida, K.-i., and Yasuda, S., 1978, A practical method for assessing soil liquefaction potential based on case studies at various sites in Japan, in 2nd International conference on microzonation, San Francisco, p. 885-896.

Iwasaki, T., Tokida, K., Tatsuoka, F., Watanabe, S., Yasuda, S., and Sato, H., 1982, Microzonation for soil liquefaction potential using simplified methods, in 3rd International Earthquake Microzonation Conference, Seattle, p. 1319-1330.

Johnston, J.W., Thompson, T.A., and Baedke, S.J., 2007, Dune and beach complex and back barrier sediments along the southeastern shore of Lake Michigan; Cowles Bog area of Indiana Dunes National Lakeshore, *in* Baker, G.S., and Jol, H.M., eds., Stratigraphic analyses using GPR: Geological Society of America Special Paper 432, p. 47-58.

Kawasumi, H., ed., 1968, General report on the Niigata earthquake of 1964: Japan, Tokyo Electrical Engineering College Press, 550 p.

Kayaballi, K., and West, T.R., 1994, Liquefaction susceptibility evaluation for the City of Evansville, Indiana: Bulletin of the Association of Engineering Geologists, v. 31, no. 2, p. 231-253.

Leon, E., Gassman, S.L., and Talwani, P., 2006, Accounting for soil aging when assessing liquefaction potential: Journal of Geotechnical and Geoenvironmental Engineering, v. 132, no. 3, p. 363-377.

Lewis, M.R., Arango, I., Kimball, J.K., and Ross, T.E., 1999, Liquefaction resistance of old sand deposits, 11th Panamerican Conference on Soil Mechanics and Geotechnical Engineering: Fo do Iguassu, Brasil, p. 821-829.

Li, D.K., Juang, C.H., Andrus, R.D., and Camp, W.M., 2007, Index properties-based criteria for liquefaction susceptibility of clayey soils: A critical assessment: Journal of Geotechnical and Geoenvironmental Engineering, v. 133, no. 1, p. 110-115.

McGowen, J.H., Brown, L.F., Jr., Evans, T.J., Fisher, W.L., and Groat, C.G., 1976, Environmental geologic atlas of the Texas Coastal Zone: Bay City - Freeport area: Texas Bureau of Economic Geology, 98 p.

McGuire, R.K., 2004, Seismic hazard and risk analysis, Earthquake Engineering Research Institute, Monograph 10, 221 p.

Moore, D.W., Lundstrom, S.C., Counts, R.C., Martin, S.L., Andrews, W.M., Jr., Newell, W.L., Murphy, M.L., Thompson, M.F., Taylor, E.M., Kvale, E.P., and Brandt, T.R., 2009, Surficial geologic map of the Evansville, Indiana, and Henderson, Kentucky area: U.S. Geolgical Survey Scientific Investigations Map 3069, scale 1:50,000.

Moss, R.E.S., Seed, R.B., Kayen, R.E., Stewart, J.P., Kiureghian, A.D., and Cetin, K., 2006, CPT-based probabilistic and deterministic assessment of in situ seismic soil liquefaction potential: Journal of Geotechnical and Geoenvironmental Engineering, v. 132, no. 8, p. 1032-1051.

Obermeier, S.F., 1989, An engineering-geologic interpretation of relict liquefaction sand features, *in* Russ, D.P., and Crone, A.J., eds., The New Madrid earthquakes: U.S. Geological Survey Professional Paper 1336-B, 114 p.

Petersen, M.D., Frankel, A.D., Harmsen, S.C., Mueller, C.S., Haller, K.M., Wheeler, R.L., Wesson, R.L., Zeng, Y., Boyd, O.S., Perkins, D.M., Luco, N., Field, E.H., Wills, C.J., and Rukstales, K.S., 2008, Documentation for the 2008 update of the United States national seismic hazard maps: U.S. Geological Survey Open-file Report 2008-1128, 61 p.

Robertson, P.K., and Wride (Fear), C.E., 1998, Evaluating cyclic liquefaction potential using the cone penetration test: Canadian Geotechnical Journal, v. 35, no. 3, p. 442-459.

Rogers, J.D., and Figuers, S.H., 1991, Site stratigraphy and near-shore development effects on soil amplification in the greater Oakland area, *in* Baldwin, J.E., II, and Sitar, N., eds., Loma Prieta Earthquake - Engineering Geology Perspectives: Association of Engineering Geologists Special Publication No. 1, p. 123-149.

Saucier, R.T., 1994a, Geomorphology and Quaternary geologic history of the Lower Mississippi Valley - Volume I: U.S. Army Engineer Waterways Experiment Station Volume I, 364 p.

Saucier, R.T., 1994b, Geomorphology and Quaternary geologic history of the Lower Mississippi Valley - Volume II: U.S. Army Engineer Waterways Experiment Station Volume II, 28 Plates p.

Saucier, R.T., and Smith, L.M., 1986, Geomorphic mapping and landscape classification of the Ouachita and Saline River Valleys, Arkanas: U.S. Army Corps of Engineers Waterways Experiment Station, Archelological Assessments Report No. 51, 11 p.

Schultz, J.R., and Krinitzsky, E.L., 1950, Geology of the lower Red River: U.S Army Corps of Engineers Waterway Experiment Station Technical Memorandum No. 3-319, 71 p.

Seed, H.B., Tokimatsu, K., Harder, L.F., and Chung, R.M., 1985, Influence of SPT procedures in soil liquefaction resistance evaluations: Journal of Geotechnical Engineering, v. 111, no. 12, p. 1425-1445.

Sowers, J.M., 1993, Creek and watershed map of Oakland and Berkeley: Oakland Museum of California.

Teller, J.T., and Leverington, D.W., 2004, Glacial Lake Agassiz: A 5000 year history of change and its relationship to the $\delta^{18}O$ record of Greenland: Geological Society of America Bulletin, v. 116, no. 5/6, p. 729-742.

Thompson, T.A., 1990, Dune and beach complex and back barrier sediments along the southeastern shore of Lake Michigan; Cowles Bog area of Indiana Dunes National Lakeshore, *in* Schneider, A.F., and Fraser, G.S., eds., Late Quaternary history of the Lake Michigan basin: Geological Society of America Special Paper 251, p. 9-20.

Thompson, T.A., and Baedke, S.J., 1997, Strandplain evidence for late Holocene lake-level variation in Lake Michigan: Geological Society of America Bulletin, v. 109, no. 6, p. 666-682.

Tinsley, J.C., Youd, T.L., Perkins, D.M., and Chen, A.T.F., 1985, Evaluating liquefaction potential, *in* Ziony, J., ed., Evaluating earthquake hazards in the Los Angeles region - an earth science perspective: U.S. Geological Survey Professional Paper 1360, p. 263-315.

Toprak, S., and Holzer, T.L., 2003, Liquefaction potential index: Field assessment: Journal of Geotechnical and Geoenvironmental Engineering, v. 129, no. 4, p. 315-322.

USDC, 1959, Future development of the San Francisco Bay area 1960-2020: U.S. Office of Area Development, U.S. Department of Commerce for the U.S. Army Engineer District, San Francisco Corps of Engineers, 94 p. p.

Van Arsdale, R., 2004a, Surficial geologic map of the Ellensdale quadrangle, Shelby County, Tennessee: U.S. Geological Survery Scientific Investigations Map 2836, scale 1:24,000.

Van Arsdale, R., 2004b, Surficial geologic map of the Germantown quadrangle, Shelby County, Tennessee: U.S. Geological Survery Scientific Investigations Map 2837, scale 1:24,000.

Weems, R.E., and Lemon, E.M., Jr., 1993, Geology of the Cainhoy, Charleston, Fort Moultrie, and North Charleston Quadrangles, Charleston and Berkeley Counties, South Carolina: U.S. Geological Survey Miscellaneous Investigations Series I-1935, scale 1:24,000.

Weems, R.E., and Lewis, W.C., 2010, Surficial geology of Charleston and parts of Berkeley, Dorchester, Colleton and Georgetown Counties, South Carolina: U.S. Geological Survey Open-file Report, scale 1:100,000 (in press).

Witter, R.C., Knudsen, K.L., Sowers, J.M., Wentworth, C.M., Koehler, R.D., and Randolph, C.E., 2006, Maps of Quaternary deposits and liquefaction susceptibility in the central San Francisco Bay region, California: U.S. Geological Survey Open-file Report 06-1037.

Youd, T.L., and Hoose, S.N., 1977, Liquefaction susceptibility and geologic setting, in 6th World Conference on Earthquake Engineering, New Delhi, India, 6th World Conference on Earthquake Engineering, Indian Society of Earthquake Technology, p. 2189-2194.

Youd, T.L., and Hoose, S.N., 1978, Historic ground failures in Northern California triggered by earthquakes, U.S. Geological Survey Professional Paper 993, 177 p.

Youd, T.L., Idriss, I.M., Andrus, R.D., Arango, I., Castro, G., Christian, J.T., Dobry, R., Finn, W.D.L., Harder, L.F., Jr., Hynes, M.E., Ishihara, K., Koester, J.P., Liao, S.S.C., Marcuson, W.F., III, Martin, G.R., Mitchell, J.K., Moriwaki, Y., Power, M.S., Robertson, P.K., Seed, R.B., and Stokoe, K.H., II, 2001, Liquefaction resistance of soils: Summary report from the 1996 NCEER and 1998 NCEER/NSF workshops on evaluation of liquefaction resistance of soils: Journal of Geotechnical and Geoenvironmental Engineering, v. 127, no. 10, p. 817-833.

Youd, T.L., and Perkins, D.M., 1978, Mapping liquefaction-induced ground failure potential: Journal of Geotechnical Engineering, v. 104, no. 4, p. 433-446.

Table 1. Study areas and geologic setting

Study Area		***Type of Geologic Deposit***	***Location***	***Geologic Map Reference***	***No. of CPT***
1		Alluvial fan	Greater Oakland, CA	Witter and others (2006)	92
2	a	Alluvial fan	Santa Clara Valley, CA	Witter and others (2006)	98
	b	Alluvial fan, young levee			25
3	a	Beach ridge (Holocene)	Greater Charleston, SC	Weems and Lewis (2010)	30
	b	Beach ridge (Pleistocene)			70
4		Beach ridge	Upper Peninsula, MI	(aerial photos)	32
5	a	Delta, topset beds	Sheyenne River, Richland County, ND	Baker (1966)	32
	b	Delta, foreset beds			19
6		Dunes, eolian	Indiana Dunes National Lakeshore, IN	Thompson (1990)	25
7	a	Floodplain (floodbasin)	Evansville, IN	Fraser and Fishbaugh (1986); Moore and others (2009)	25
	b	Floodplain (natural levee)			13
8	a	Floodplain (point bar)	Mississippi River, AK, MO, and MS	Saucier (1994b)	90
	b	Floodplain (abandoned channel)			40
	c	Floodplain (floodbasin)			20
9		Floodplain (point bar)	Ouachita River, AK	Saucier and Smith (1986)	30
10		Floodplain (point bar)	Red River, AK	Schultz and Krinitizsky (1950)	30
11		Floodplain (point bar)	Rio Grande, TX	Brown et al. (1980)	32
12		Floodplain (point bar)	Wolf River, TN	Broughton (1999); Cox (2004); Van Arsdale (2004a, b)	23
13		Lacustrine	Richland County, ND	Baker (1966)	25
14		Lagoonal	Brazoria and Matagorda Counties, TX	Fisher and others (1972); McGowen and others (1976)	30
15		Sandy artificial fill	Greater Oakland, CA	Witter and others (2006)	82
16		Valley train, Pvl1	Mississippi Valley, AK and MO	Saucier (1994b)	37
		Valley train, Pvl2			35

Table 2. Drainage areas

River	Drainage Area	
	mi^2	km^2
Mississippi River at Memphis, TN	932,800	2,414,908
Rio Grande, TX	182,000	471,176
Red River at Fulton, AR	46,444	120,238
Ouachita River at Camden, AR	5,357	13,869
Wolf River, TN	709	1,836

Table 3. Constants for logistic

Study Area	Type of Geologic Deposit	Location	WT=1.5m			WT=5m		
			a	b	c	a	B	c
1	Alluvial fan	Greater Oakland, CA	0.0479	0.3233	-6.0539	0	—	—
2	Alluvial fan	Santa Clara Valley, CA	1.8336	1.2479	-2.5577	0.2268	0.6571	-3.4305
	Alluvial fan, young levee		0.6503	0.2981	-3.7789	0.5886	0.4586	-3.5751
3	Beach ridge (Holocene)	Greater Charleston, SC	0.9542	0.1861	-3.8421	0.9382	0.2530	-4.2631
	Beach ridge (Pleistocene)		0.9903	0.2503	-7.4332	0.8520	0.3475	-6.4186
4	Beach ridge	Upper Peninsula, MI	0.5648	0.3872	-5.8965	2.1841	1.2806	-3.3766
5	Delta, topset beds	Sheyenne River, Richland County, ND	0.9759	0.2530	-8.0436	0.9236	0.3192	-8.0451
	Delta, foreset beds		0.3498	0.4307	-9.5162	0	—	—
6	Dunes, eolian	Indiana Dunes National Lakeshore, IN	0.8915	0.2510	-5.1627	0.6635	0.3584	-5.3073
7	Floodplain (floodbasin)	Evansville, IN	0.3405	0.3705	-2.3085	0.0699	0.2244	-5.5514
	Floodplain (levee)		1.0802	0.2741	-2.7483	1.7482	0.7912	-1.9527
8	Floodplain (point bar)	Mississippi River, AK, MO, and MS	0.9514	0.2231	-4.7039	0.8717	0.3339	-5.2697
	Floodplain (aban. chan.)		0.7781	0.2107	-5.7692	0.6539	0.2858	-5.5505
	Floodplain (floodbasin)		0.6018	0.2397	-3.2337	0.5062	0.3226	-3.9267
9	Floodplain (point bar)	Ouachita River, AK	1.0023	0.1940	-4.1876	0.9702	0.3372	-4.3742
10	Floodplain (point bar)	Red River, AK	0.9741	0.2370	-6.7458	0.9671	0.3417	-7.1810
11	Floodplain (point bar)	Rio Grande, TX	0.8479	0.2743	-6.5802	0.8056	0.4038	-7.1731
12	Floodplain (point bar)	Wolf River, TN	1.0079	0.2924	-4.8917	0.8432	0.4223	-6.4632
13	Lacustrine	Richland County, ND	0.0707	0.4644	-12.2006	0	—	—
14	Lagoonal	Brazoria and Matagorda Counties, TX	0.7539	0.2383	-4.3654	0.6221	0.3571	-4.3517
15	Sandy artificial fill	Greater Oakland, CA	0.7835	0.2319	-4.6302	0.4421	0.3972	-3.4154
16	Valley train, Pvl1	Mississippi Valley, AK and MO	1.0155	0.2784	-6.8479	0.8240	0.3988	-3.4256
	Valley train, Pvl2		0.8816	0.3084	-3.1019	0.9858	0.4176	-6.9698

Table 4. Probability ranges for Youd and Perkins (1978) susceptibilities

Susceptibility	Probability Range		
	M7.5, PGA=0.25 g, WT=1.5 m	**M**7.5, PGA=0.25 g, WT=5.0 m	**M**6.0, PGA=0.25 g, WT=1.5 m
Very low	0	0	0
Low	<0.08	<0.04	<0.02
Moderate	0.08-0.30	0.04-0.14	0.02-0.07
High	0.30-0.62	0.14-0.20	0.07-0.14
Very high	>0.62	>0.20	>0.14

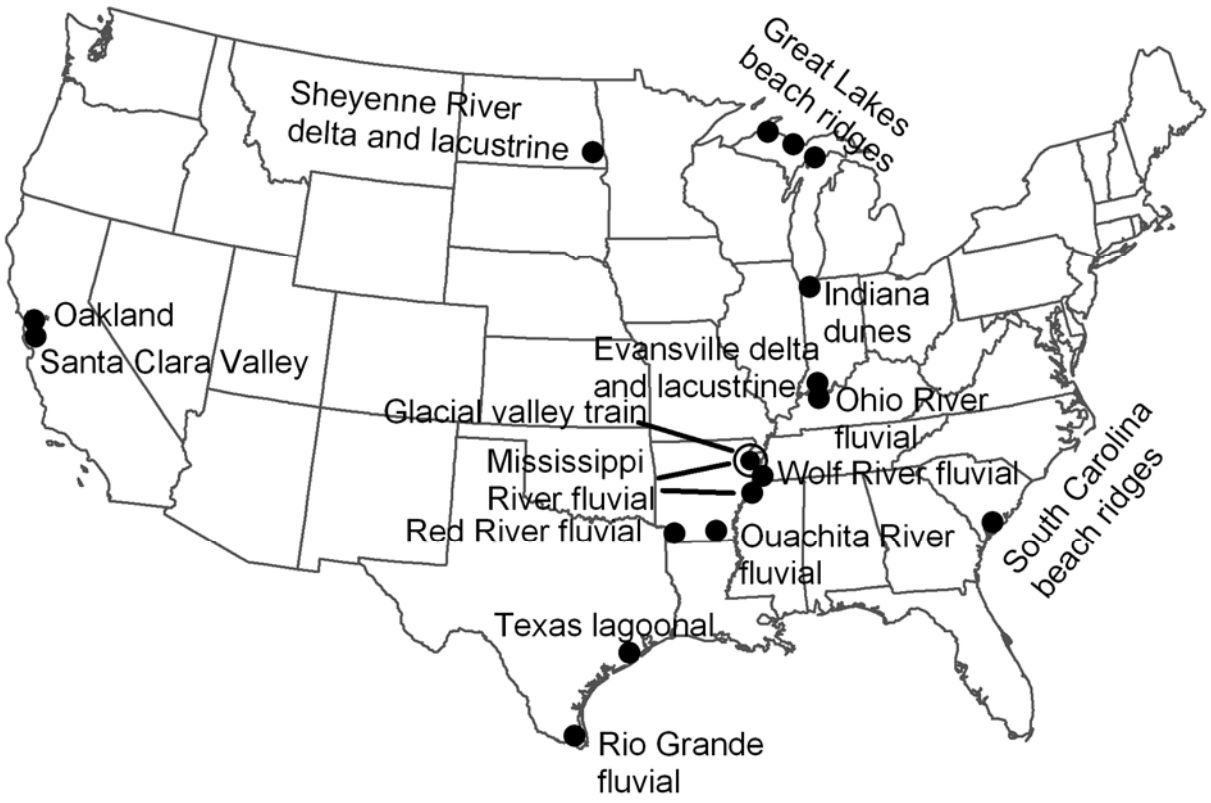

Figure 1. Map showing study areas in conterminous United States.

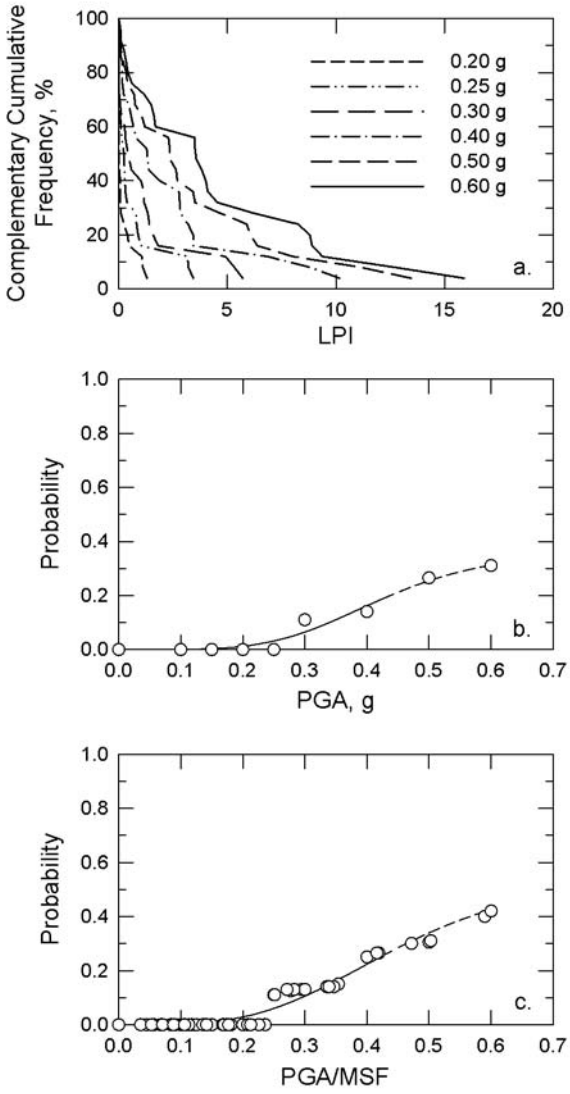

Figure 2. Illustration of methodology to compute liquefaction probability. a. Complementary cumulative frequencies of LPI are computed for a given seismic loading (**M**7) and water table depth (WT = 5.0 m); b. Probabilities are the frequency from (a) at LPI = 5; and c. Seismic demand (PGA) is scaled for earthquake magnitude by dividing MSF. Modified from (Holzer and others, 2009).

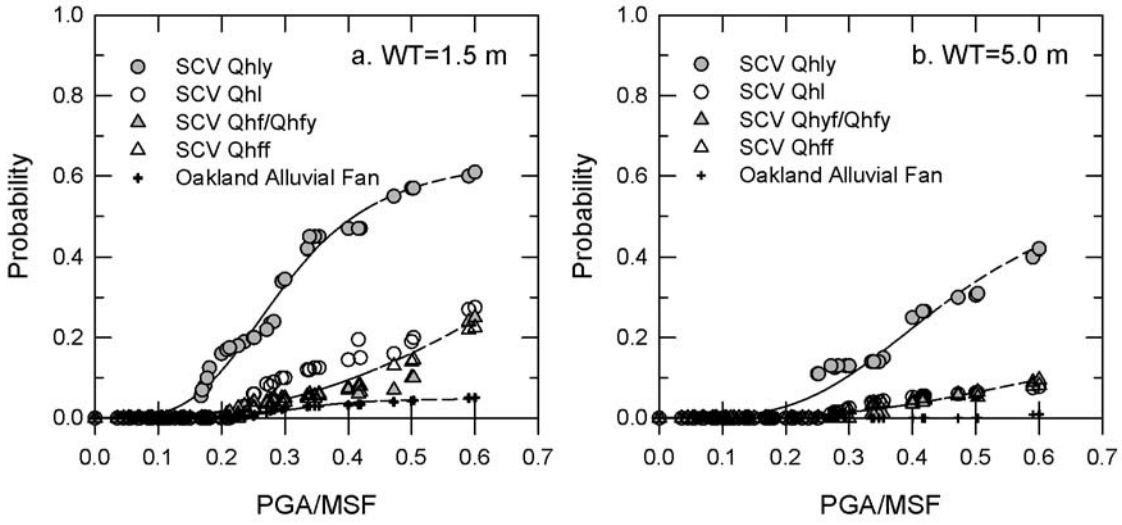

Figure 3. Liquefaction probability curves for alluvial fan deposits (Areas 1 and 2): a. WT = 1.5 m; and b. WT = 5.0 m.

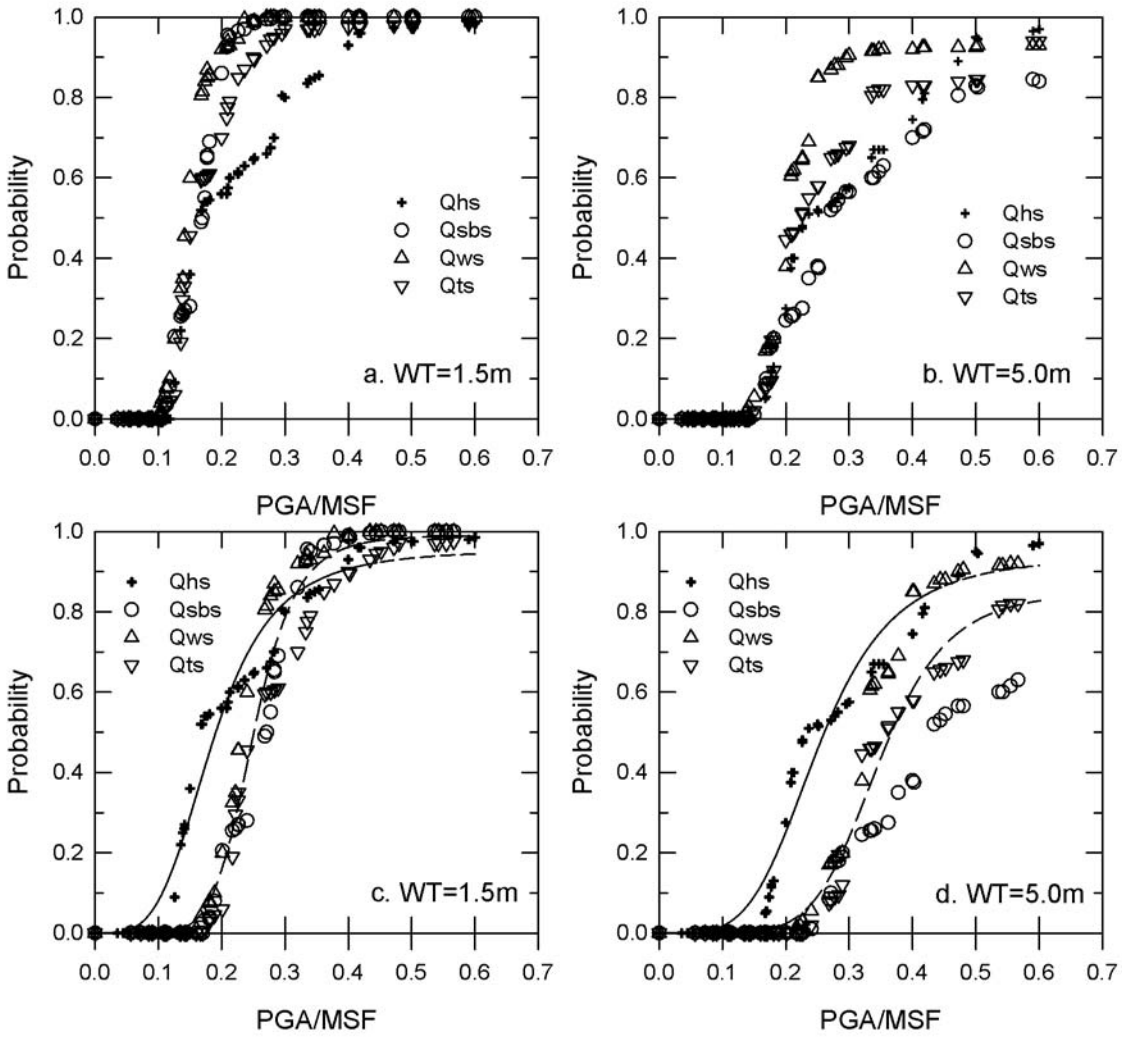

Figure 4. Liquefaction probability curves for South Carolina beach ridges (Area 3). a. WT=1.5 m; b. WT=5.0 m; c. WT=1.5 m with a 1.6 aging factor applied to Pleistocene beach ridges; d. WT=5.0 m, with a 1.6 aging factor applied to Pleistocene beach ridge. Solid line is the logistic fit to the Holocene beach ridge; dashed line is logistic fit to all three Pleistocene beach ridges. Qhs is the modern beach ridge complex, and the ages of beach ridge complexes Qsbs, Qws, and Qts, respectively, are 33,000 to 85,000, 70,000 to 130,000, and 200,000-240,000 yr (Weems and Lemon, 1993).

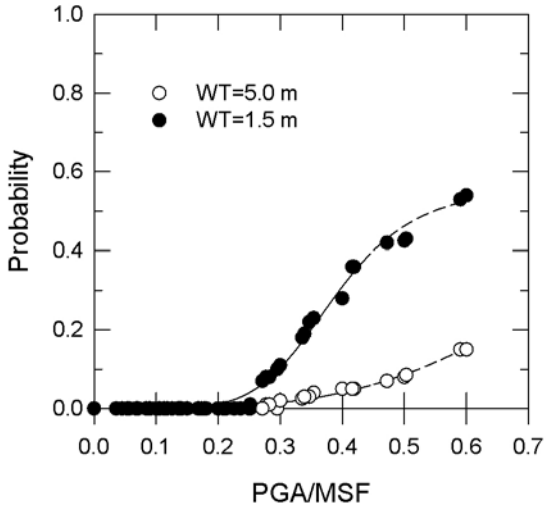

Figure 5. Liquefaction probability curves for Great Lakes beach ridges (Area 4).

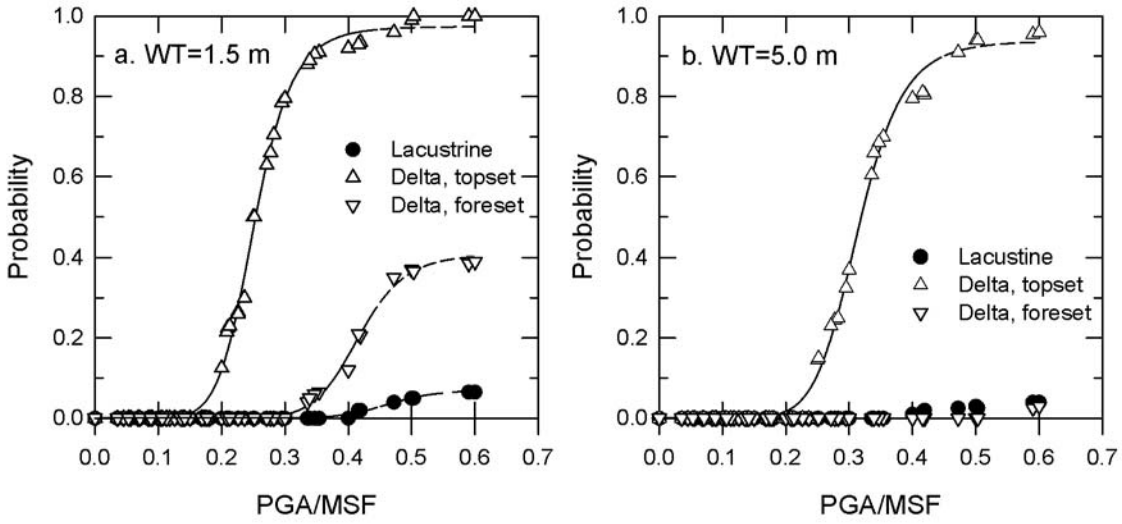

Figure 6. Liquefaction probability curves for deltaic topset and foreset bed deposits and deep-water lacustrine deposits for Lake Agassiz, Richland Country, North Dakota (Areas 5 and 14). a. WT = 1.5 m; and b. WT = 5.0 m.

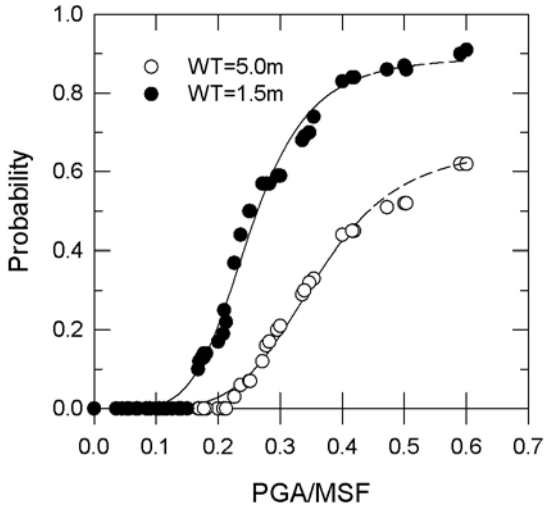

Figure 7. Liquefaction probability curves for eolian (wind-blown) dunes (Area 6). a. WT = 1.5 m; and b. WT = 5.0 m.

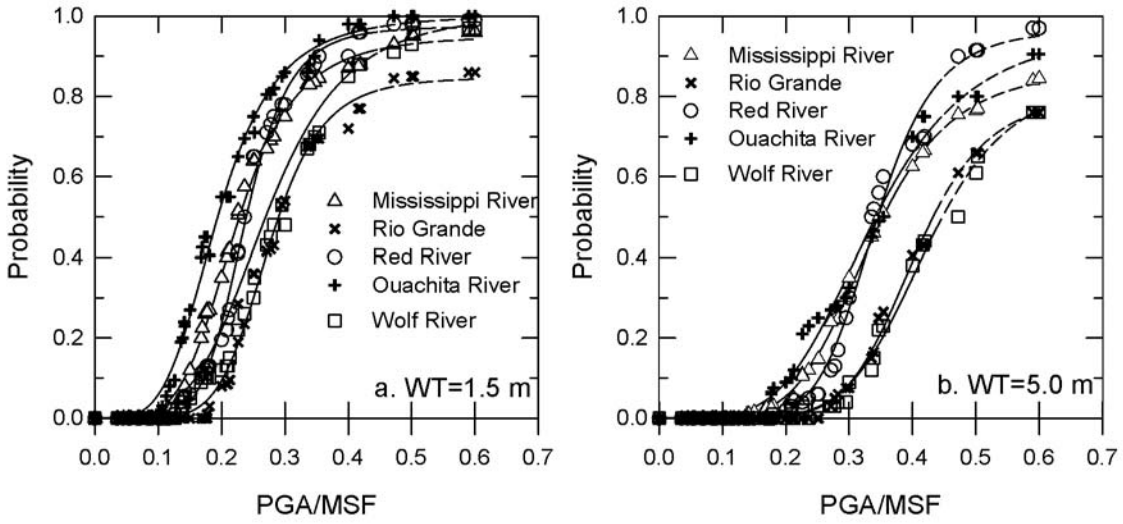

Figure 8. Liquefaction probability curves for floodplain point bar deposits (Areas 8, 9, 10, 11, and 12). a. WT = 1.5 m; and b. WT = 5.0 m.

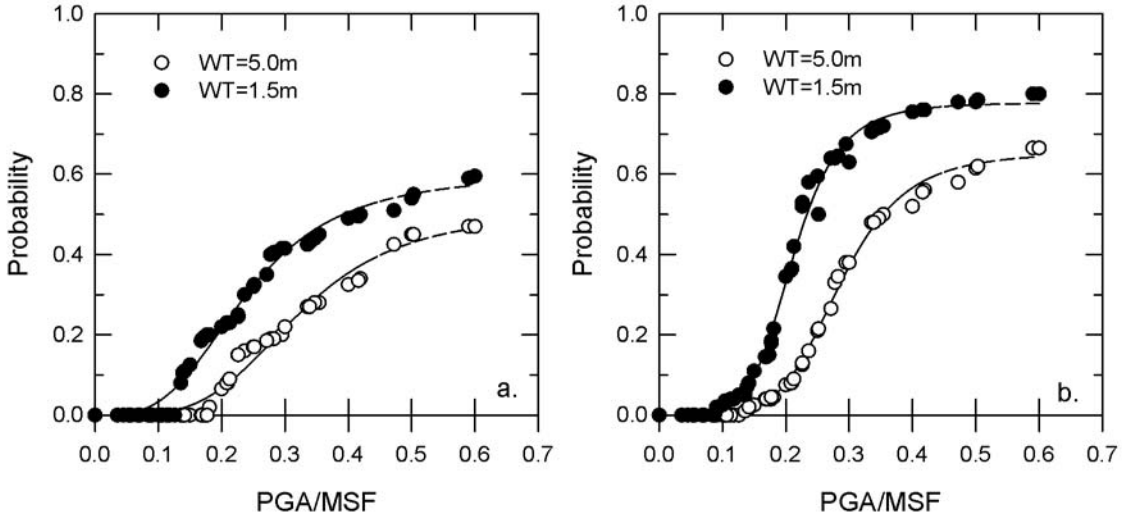

Figure 9. Liquefaction probability curves for Mississippi River (Area 8). a. floodbasin deposits; and b. abandoned channel deposits.

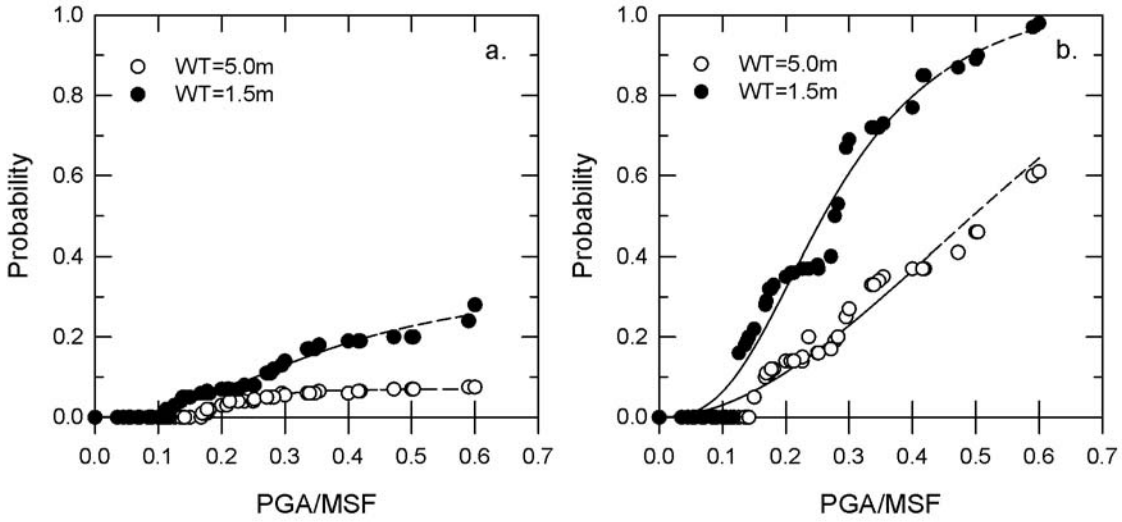

Figure 10. Liquefaction probability curves for Evansville, IN, Ohio River (Area 7). a. floodbasin deposits; and(b) natural levee deposits.

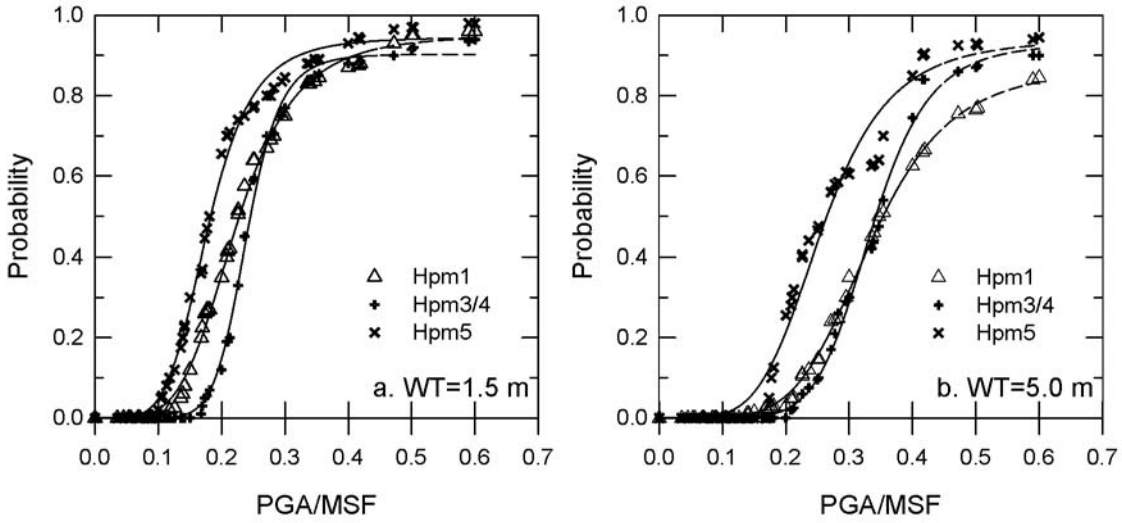

Figure 11. Evaluation of aging of Holocene point bar deposits, Mississippi River (Area 8). a. WT = 1.5 m; and b. WT = 5.0 m. Hpm1 underlies the modern floodplain and is as less than 3,000 yr old; Hpm3/Hpm4 ranges in age from 6,500 to 3,800 yr; and Hpm5 ranges in age from 9,200 to 7,000 yr (Saucier, 1994a).

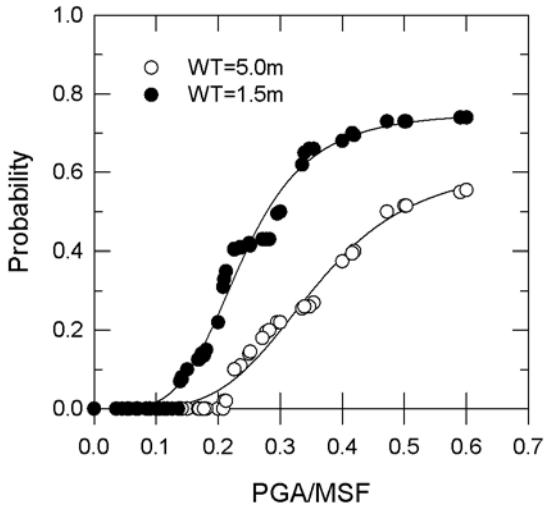

Figure 12. Liquefaction probability curves for lagoonal deposits, Texas Gulf Coast (Area 14).

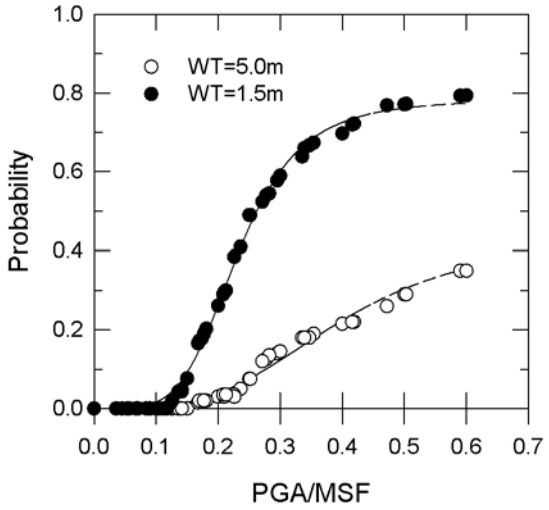

Figure 13. Liquefaction probability curves for sandy artificial fill, east bay, greater Oakland area, San Francisco Bay, CA (Areas 15).

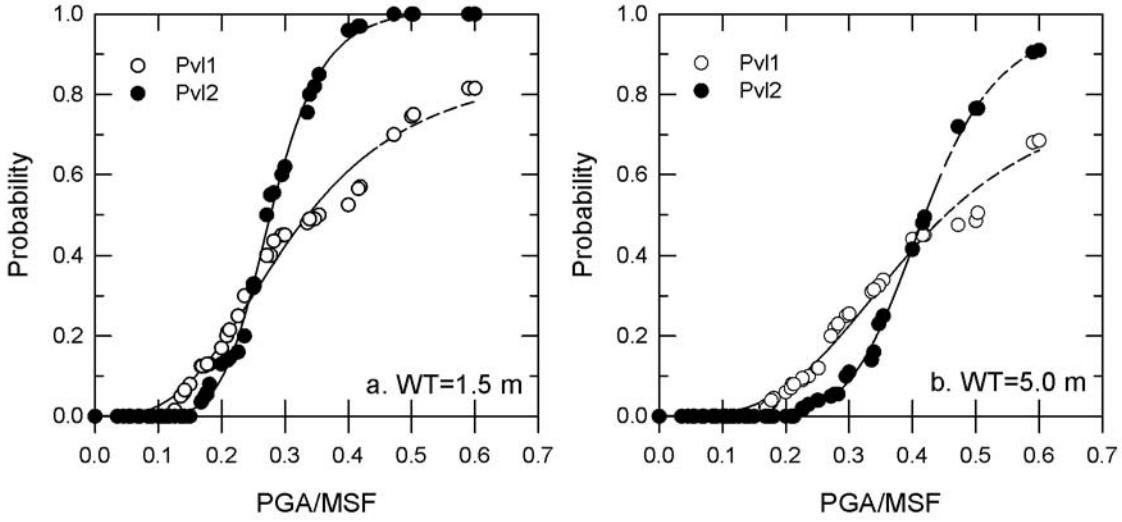

Figure 14. Liquefaction probability curves for valley train deposits, Mississippi River Valley (Area 16). a. WT = 1.5 m; and b. WT = 5.0 m.

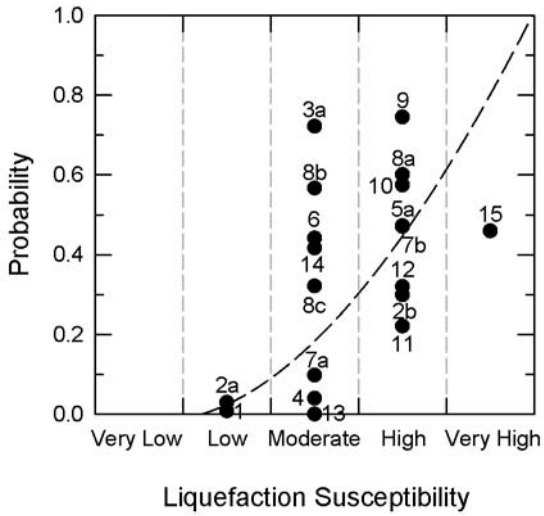

Figure 15. Computed probabilities of surface manifestations of liquefaction versus liquefaction susceptibility proposed by Youd and Perkins (1978). Probabilities are for an **M**7.5 earthquake with a PGA=0.25 g and a water table depth of 1.5 m. See Table 1 to identify data labels.